The Dynamics of the Pacific-North America Plate Boundary Zone since the Oligocene

STONY BROOK UNIVERSITY

William Holt
Ali Bahadori
Troy Rasbury
Laurent Montessi

The time-dependent strain rate field for the southwestern North American Lithosphere Since 36 Ma

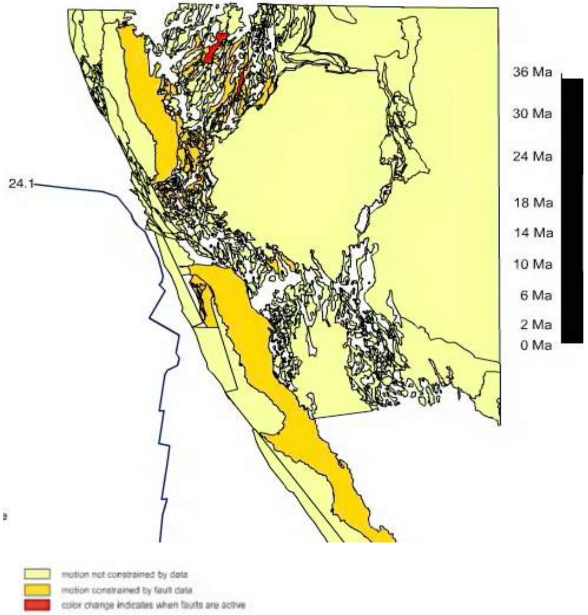

McQuarrie and Wernicke, 2005, An Animated Tectonic Reconstruction of Southwestern North America since 36 MA: Geosphere, v. 1, no.3, doi: 10.1130/GES00016.1

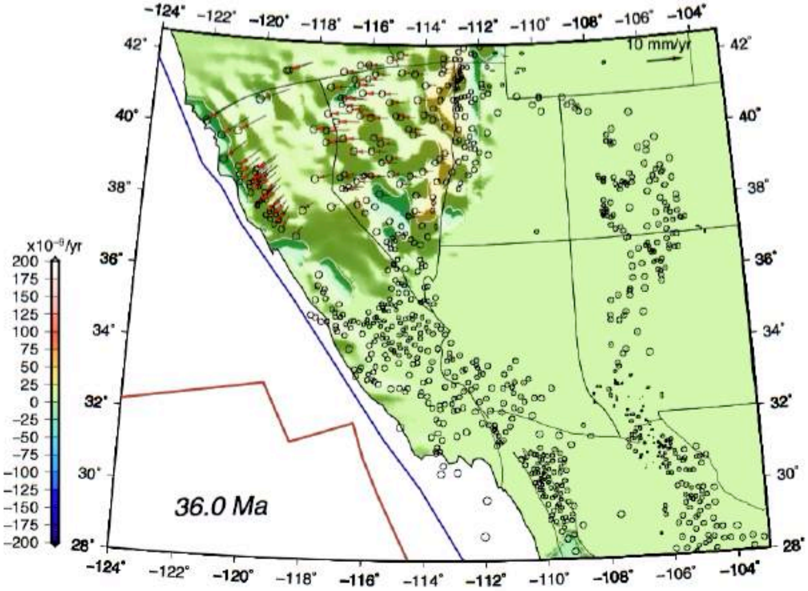

Contours of dilatational strain rates of western U.S. from 36 Ma to present-day (Bahadori et al., 2018) **Geosphere**

Reconstruction of Crustal Thickness Evolution in Western U.S.

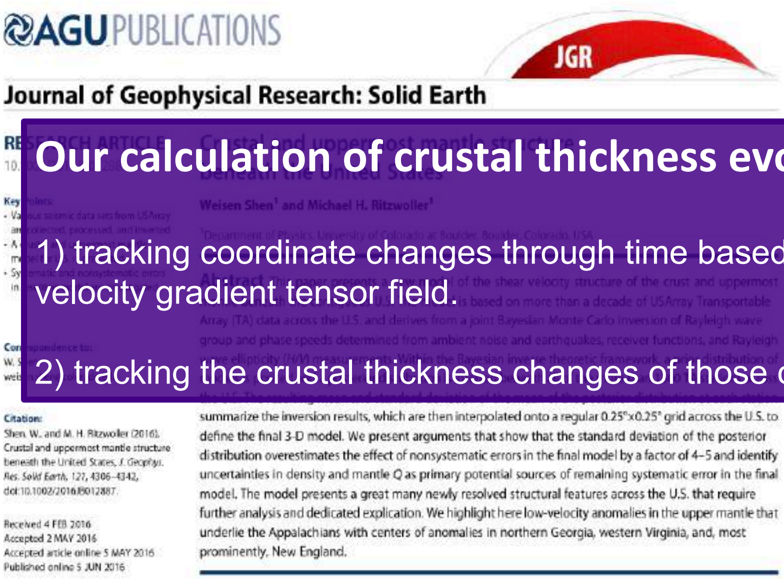
AGU PUBLICATIONS

JGR

Journal of Geophysical Research: Solid Earth

Weisen Shen[1] and Michael H. Ritzwoller[1]

[1]Department of Physics, University of Colorado at Boulder, Boulder, Colorado, USA

Abstract This paper presents a new model of the shear velocity structure of the crust and uppermost mantle beneath the U.S. ... is based on more than a decade of USArray Transportable Array (TA) data across the U.S. and derives from a joint Bayesian Monte Carlo inversion of Rayleigh wave group and phase speeds determined from ambient noise and earthquakes, receiver functions, and Rayleigh wave ellipticity (H/V) measurements. Within the Bayesian inverse theoretic framework, a prior distribution of ...

... the U.S. The resulting mean and standard deviation of the mean of the posterior distribution at each station summarize the inversion results, which are then interpolated onto a regular 0.25°x0.25° grid across the U.S. to define the final 3-D model. We present arguments that show that the standard deviation of the posterior distribution overestimates the effect of nonsystematic errors in the final model by a factor of 4–5 and identify uncertainties in density and mantle Q as primary potential sources of remaining systematic error in the final model. The model presents a great many newly resolved structural features across the U.S. that require further analysis and dedicated explication. We highlight here low-velocity anomalies in the upper mantle that underlie the Appalachians with centers of anomalies in northern Georgia, western Virginia, and, most prominently, New England.

Citation:
Shen, W., and M. H. Ritzwoller (2016), Crustal and uppermost mantle structure beneath the United States, J. Geophys. Res. Solid Earth, 121, 4306–4342, doi:10.1002/2016JB012887.

Received 4 FEB 2016
Accepted 2 MAY 2016
Accepted article online 5 MAY 2016
Published online 5 JUN 2016

Our calculation of crustal thickness evolution involves:

1) tracking coordinate changes through time based on the time-dependent horizontal velocity gradient tensor field.

2) tracking the crustal thickness changes of those corresponding coordinates.

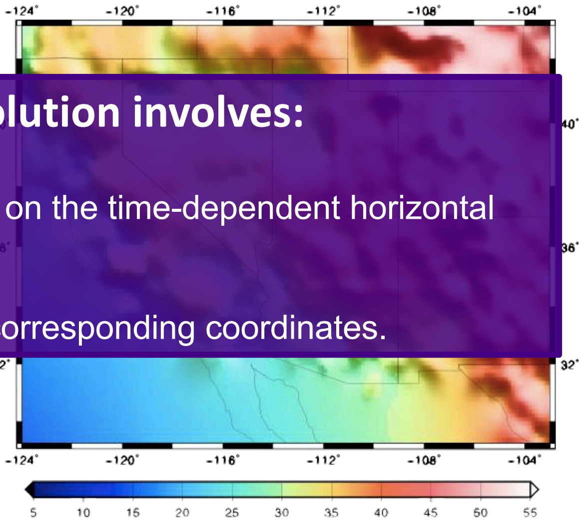

present day model of western U.S. crustal thickness in km from *Shen and Ritzwoller (2016)*.

Finite Strain Estimate Inferred From Distribution of Vertical Strain

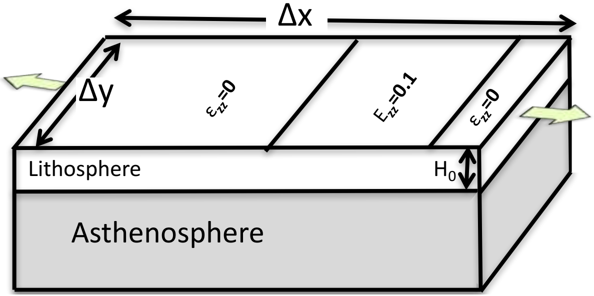

Instantaneous strain rate distribution

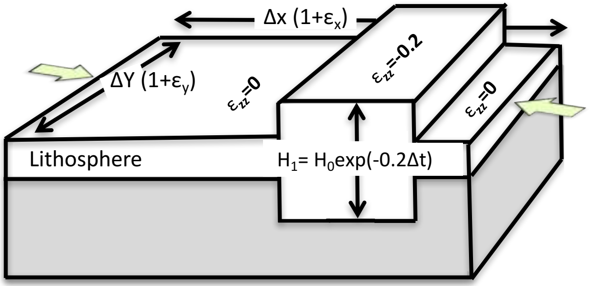

Assumptions:

1) We approximate zero volume change, and thus the vertical strain rates $\epsilon_{zz} = -(\epsilon_{xx}+\epsilon_{yy})$.

2) We assume that the lithosphere deformation is vertically coherent.

3) We ignore erosion and igneous input

Finite Strain Estimate Inferred From Distribution of Vertical Strain

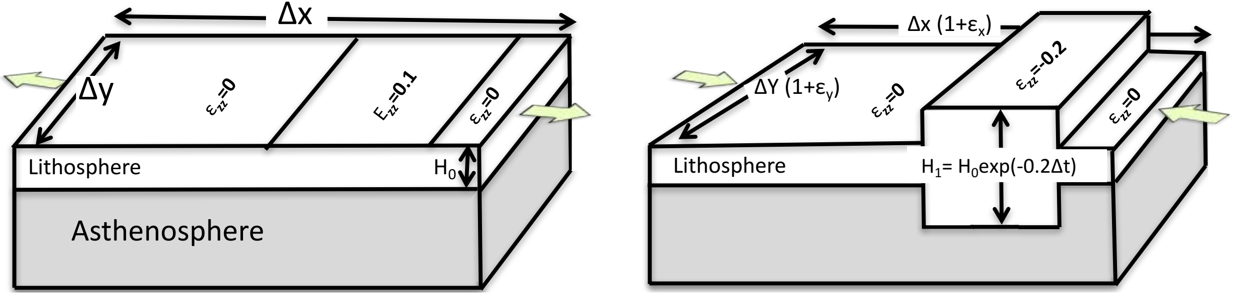

Instantaneous strain rate distribution

$$\frac{dF}{dt} = LF \longrightarrow H_{old} = H_{young} \exp(-\mathring{\varepsilon}_{zz} \Delta t)$$

Mckenzie and Jackson (1983)

Western U.S. Crustal Thickness Evolution Vs. Time

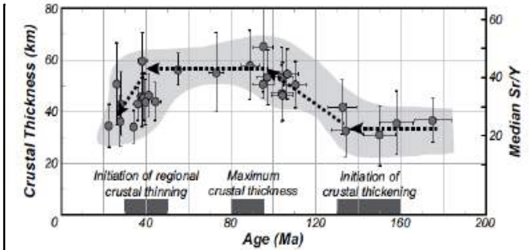

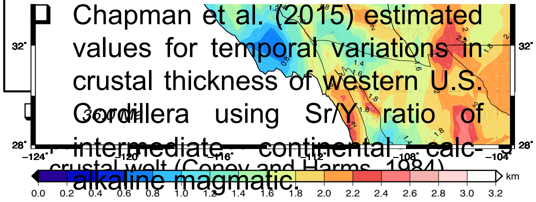

- Chapman et al. (2015) estimated values for temporal variations in crustal thickness of western U.S. Cordillera using Sr/Y ratio of intermediate continental calc-alkaline magmatic.
- Contour map of standard error estimates (km) of crustal thickness for the Basin and Range of the western United States at 36 Ma.

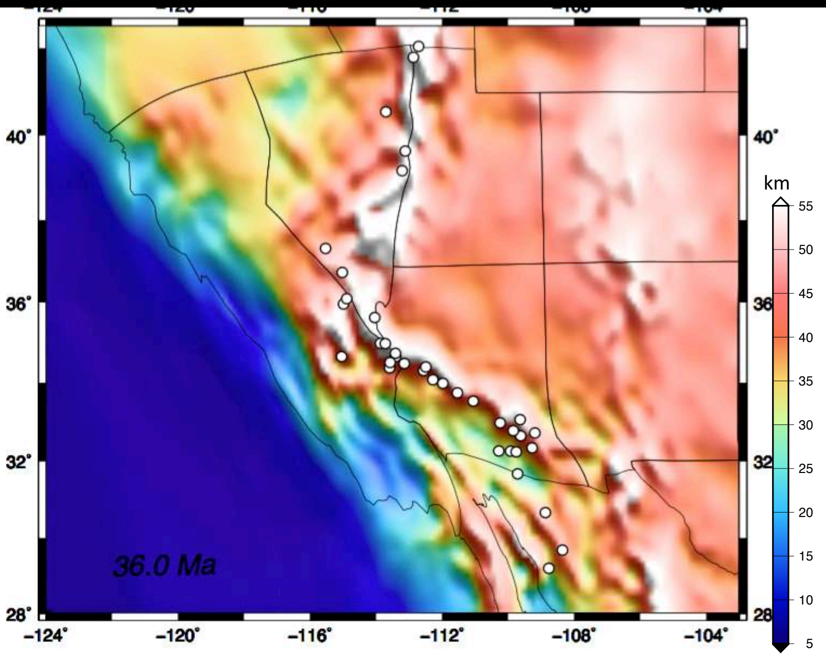

White circles are reconstructed position of Metamorphic Core Complexes (MCCs) (Bahadori et al., 2018) **Geosphere**

Influence of Thermal Perturbations on Western U.S. Upper Mantle Densities

- Using the Laplace equation and assuming constant thermal conductivity, the steady-state conductive heat distribution with no heat generation is:

$$\partial^2 T / \partial x^2 + \partial^2 T / \partial y^2 = 0$$

- Using the Fourier equations, then the heat flow (Q) in the x and y directions is calculated as:

$$Q_x = -k_A \, \partial T_{i(x)} / \partial x$$
$$Q_y = -k_A \, \partial T_{i(y)} / \partial y$$

- Based on thermal expansion of upper mantle at constant pressure and differential temperatures the new time and temperature dependent upper mantle is produced as:

$$\rho_T(\phi_{k-1}, \theta_{k-1}) = \rho_T(\phi_k, \theta_k) / [1 + \alpha \times \Delta T(\phi_{k-1}, \theta_{k-1})]$$

(Bahadori et al., 2018) **Geosphere**

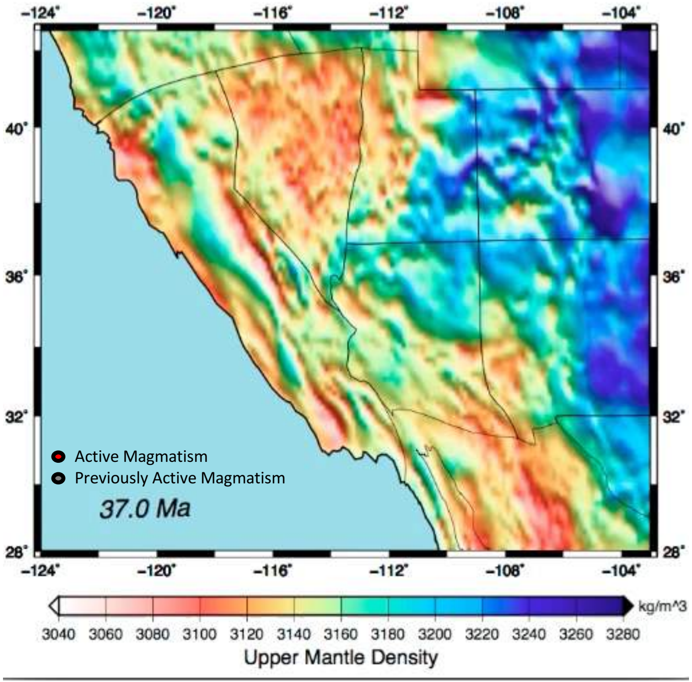

The Correlation of Ignimbrite Flare-up with collapse

- Final integrated topography model shows a highland with an average elevation of ~3.9 ± 0.3 km in central, eastern, and southern Nevada, western Utah, parts of easternmost California, and for northwestern Arizona. The Mogollon Highlands are also present within central and southeastern Arizona at 36 Ma.

(Bahadori et al., 2018) **Geosphere**

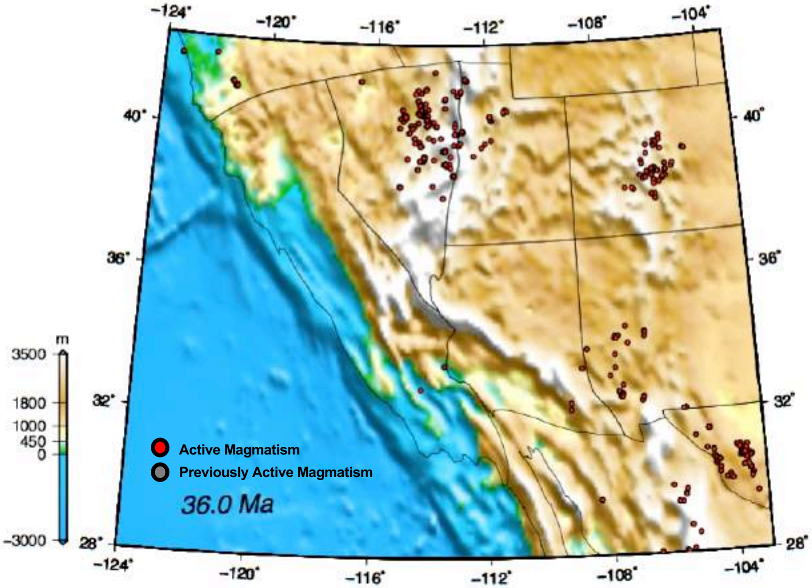

Paleoelevation evolution of western U.S. from 36 Ma to present-day. Red and gray dots are the reconstructed positions of present-day coordinates of magmatism in western U.S. (*Bahadori et al., 2018*)

Force Balance Solution – GPE gradients

$$\frac{\partial \sigma_{ij}}{\partial x_j} + \rho g_i = 0$$

England and Molnar (1997)

$$\bar{\sigma}_{zz} = -\int_{-h}^{L}\left[\int_{-h}^{z}\rho(z')g\,dz'\right]dz = -\int_{-h}^{L}(L-z)\rho(z)g\,dz$$

$$\frac{\partial}{\partial x_\beta}\left(\bar{\tau}_{\alpha\beta} + \delta_{\alpha\beta}\bar{\tau}_{\gamma\gamma}\right) = -\frac{\partial \bar{\sigma}_{zz}}{\partial x_\alpha}$$

Flesch et al. (2001)

Spatial Changes in Deviatoric Stress ↔ Spatial Changes in Gravitational Potential Energy (GPE)

What is the state of deviatoric stress that generated the collapse?

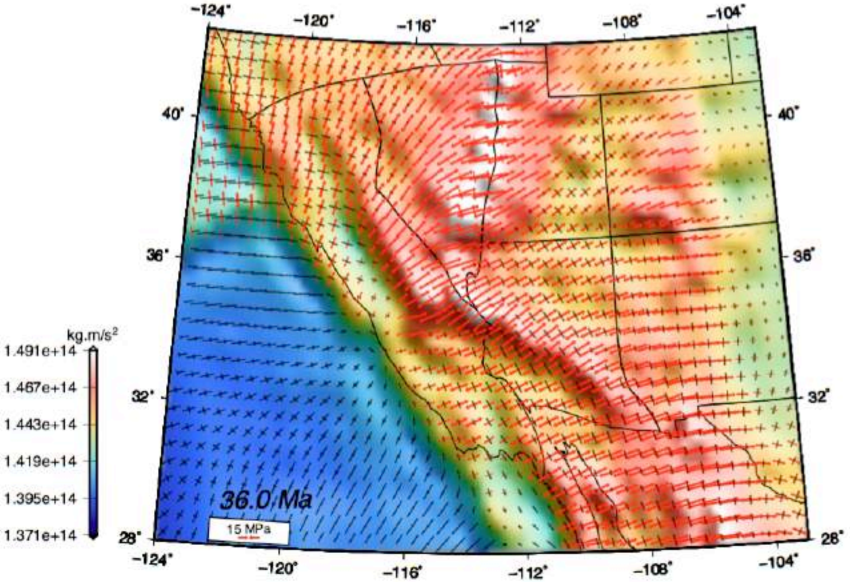

Vertically integrated deviatoric stresses associated with GPE differences

Depth Integrated Forward Dynamic Deviatoric Stresses

1) Invert for stress boundary conditions. Observations = kinematic tensor field

2) Apply Forward model using velocity boundary conditions, GPE gradients (body forces), laterally varying effective Viscosity (T/E) from inverse model. Method outlined in Flesch et al. (2001)

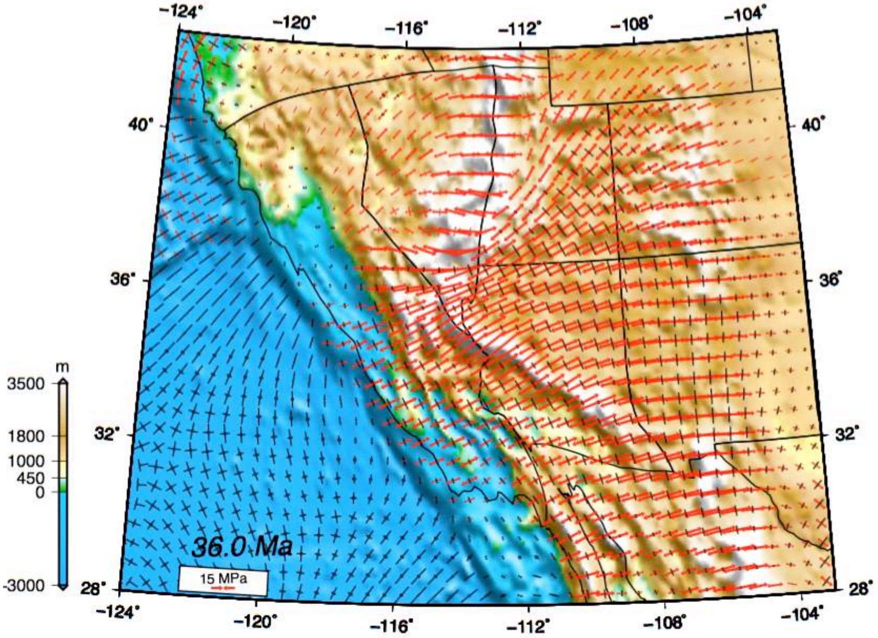

GPE Deviatoric Stresses + Stress Field Boundary Conditions

What do boundary condition solutions represent? Answer = coupling with global mantle flow

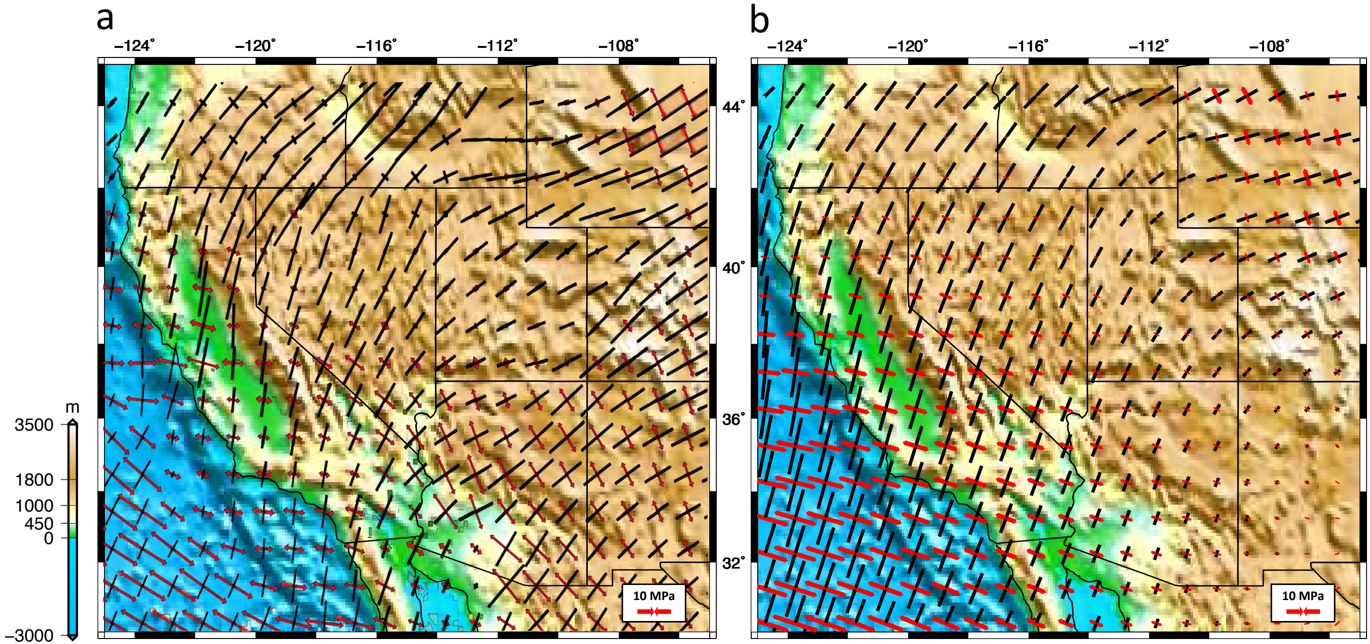

Deviatoric stresses from lithosphere coupling with global mantle flow S40RTS (Wang et al., 2015)

Best fit boundary condition solution of deviatoric stresses at 0 Ma

SH11_TX2008^{s_127}

[*Becker*, 2012; *Schmandt and Humphreys*, 2010; *Schmandt and Humphreys*, 2011; *Simmons et al.*, 2009]

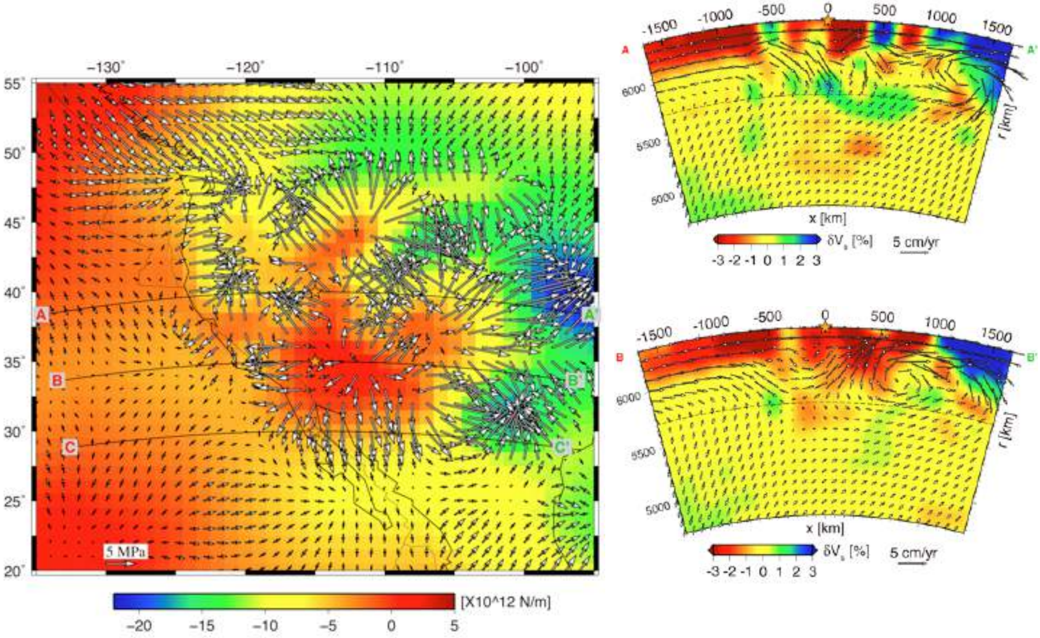

SH11_TX2008s_127

[*Becker*, 2012; *Schmandt and Humphreys*, 2010; *Schmandt and Humphreys*, 2011; *Simmons et al.*, 2009]

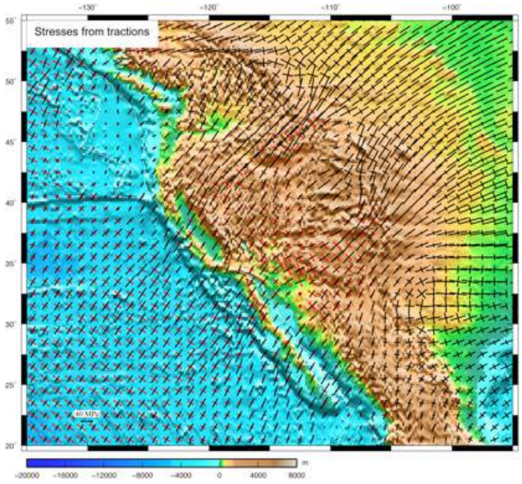

Stresses from Mantle Flow Associated Tractions

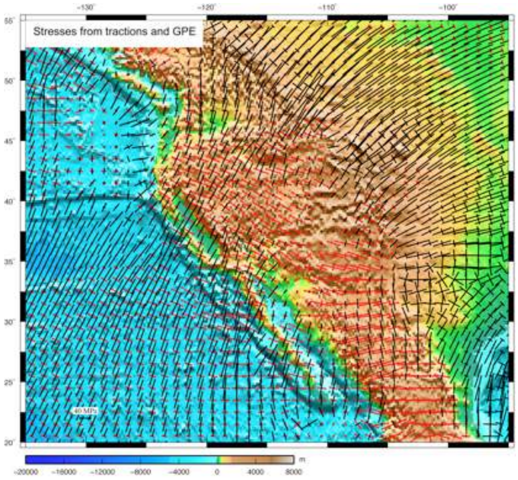

Total Stresses from Mantle Flow + GPE Gradients

Forward Dynamic Model Compared with stretch directions from core complexes, Miocene faults and dikes

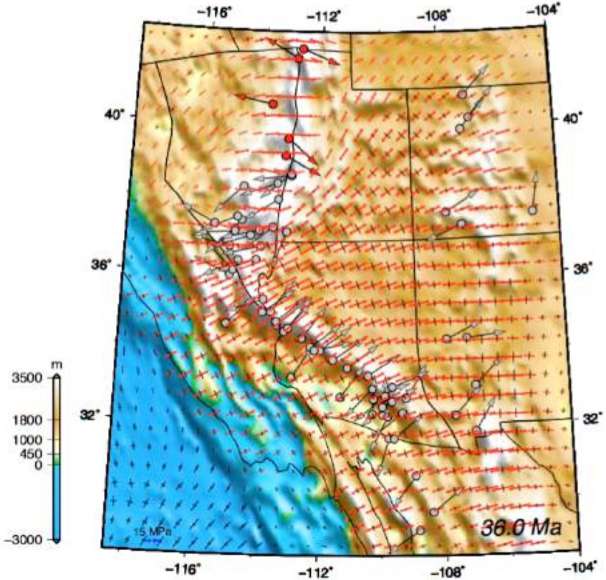

The Role of GPE For Driving the Extensional Collapse of the Western U.S.

$$\frac{T_{GPE}}{T_{Boundary}}$$

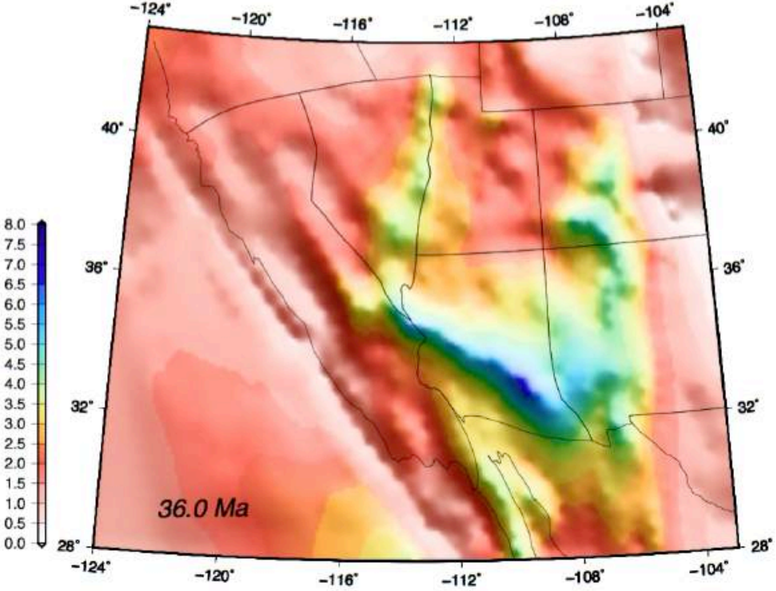

Forward Dynamic Model Velocities Compared with Kinematic Model Velocities

Forward model: velocity boundary conditions, GPE gradients (body forces), laterally varying effective Viscosity (T/E) from inverse model

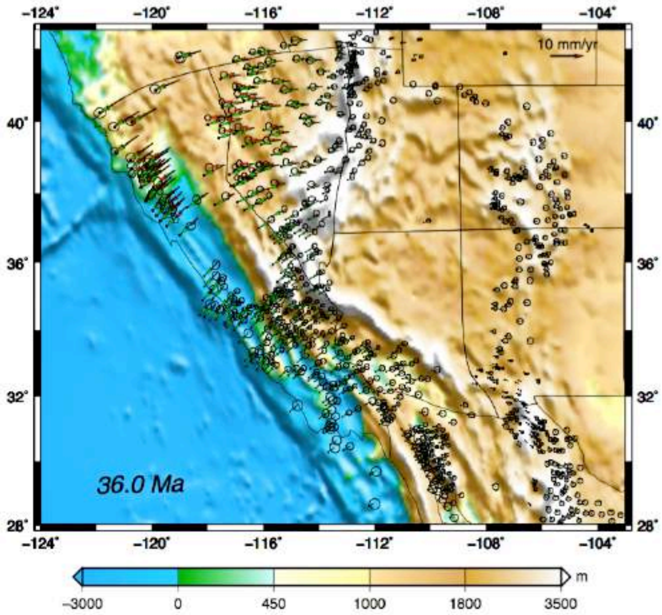

Effective Viscosity of Lithosphere in Western U.S. from Forward Dynamic Model

$$\overrightarrow{\eta}_{effective} = \frac{T}{E}$$

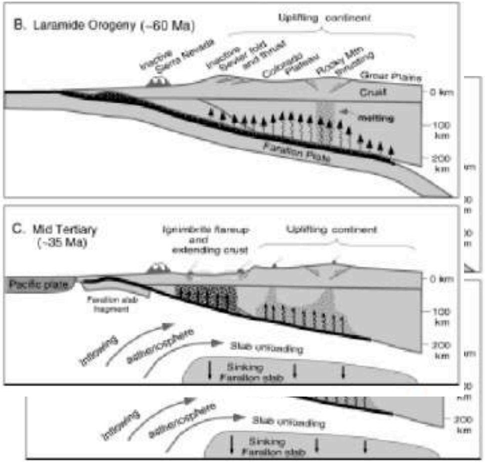

Hydration hypothesis for Laramide and mid-Tertiary magmatism, tectonism and uplift for western U.S. (*Humphrey et al., 2003*).

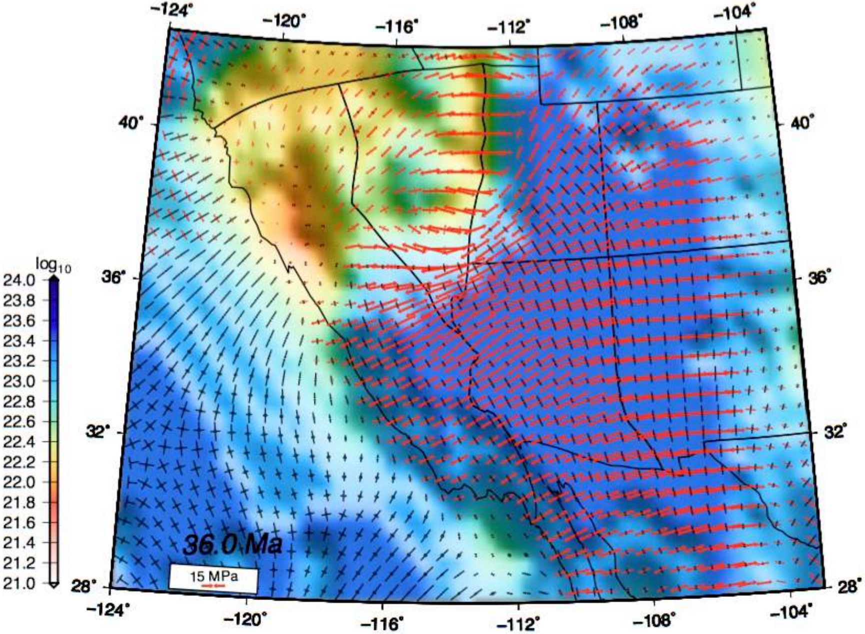

Depth integrated effective viscosity of the lithosphere in western U.S. from 36 Ma to present-day.

Computation of Lithospheric Effective Water Content Variation in Western U.S.

$$\eta_{eff} = \dot{\varepsilon}^{\left(\frac{1-n}{n}\right)} A^{\frac{-1}{n}} C_{OH}^{\frac{-r}{n}} \left[\exp\left(-\frac{(H+PV)}{RT}\right)\right]^{\frac{-1}{n}} 10^6$$

Dixon et al. (2004)

η_{eff}: effective viscosity
ε: strain rate
n: stress exponent (3.5)
r: fugacity exponent (1.2)
R: gas constant
H: activation enthalpy
H = Q + PV (Q: activation energy, V: volume, P: pressure)
T: temperature
A: material constant
n, A, Q and V were determined experimentally for the given material (olivine) (*Dixon et al., 2004*).

- The upper mantle is primarily composed of olivine, which is known to be weakened by water, thus increasing the strain rate.

- Nominally anhydrous minerals (including olivine) may have a significant effect on the viscosity and rheology of the upper mantle.

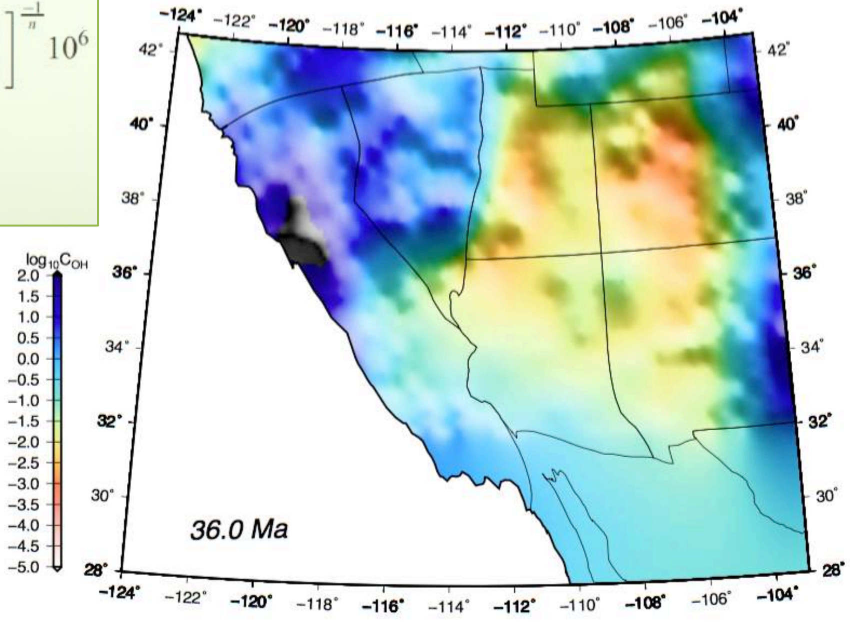

Estimate of water content (C_{OH}) at 60 km depth in western U.S.

Velocity and strain rate field from forward dynamic model (velocity boundary conditions, GPE gradients, laterally varying effective viscosity).

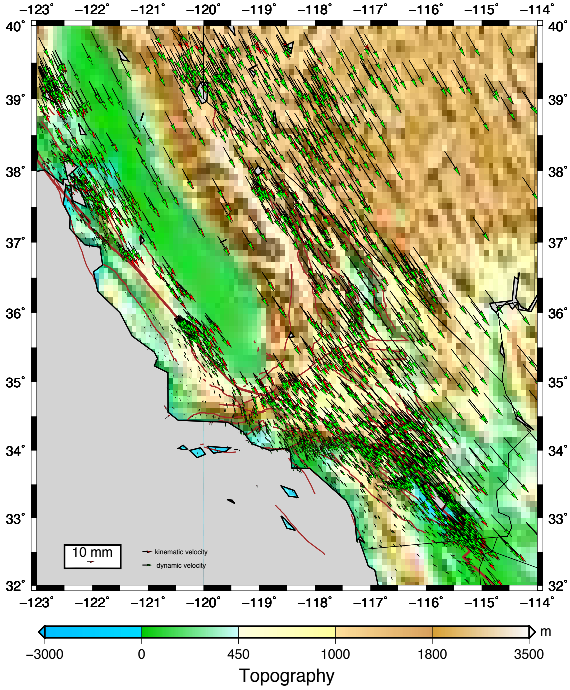

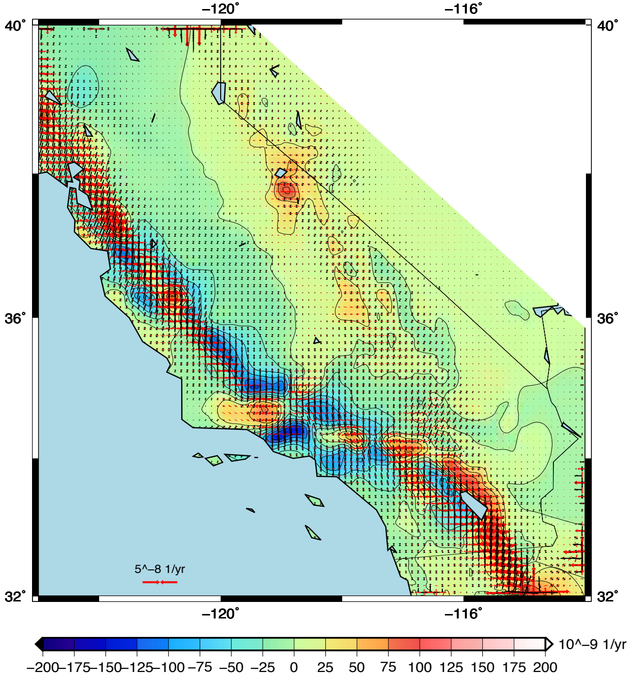

Vertically averaged effective viscosities and velocity residuals (dynamic vs. GPS – Pacific frame)

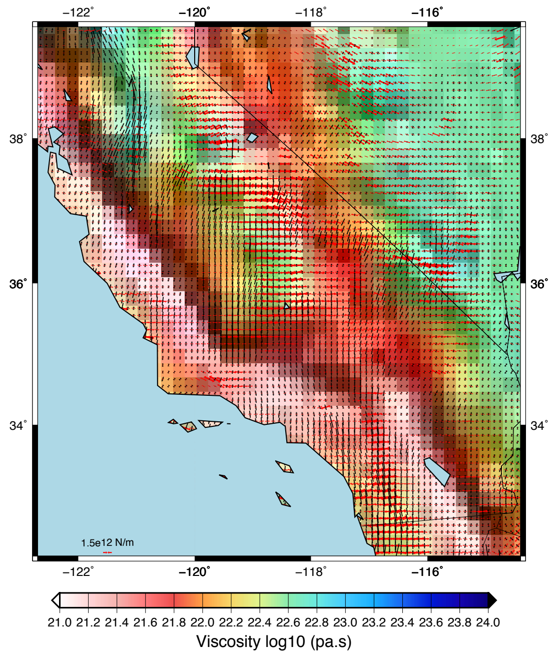

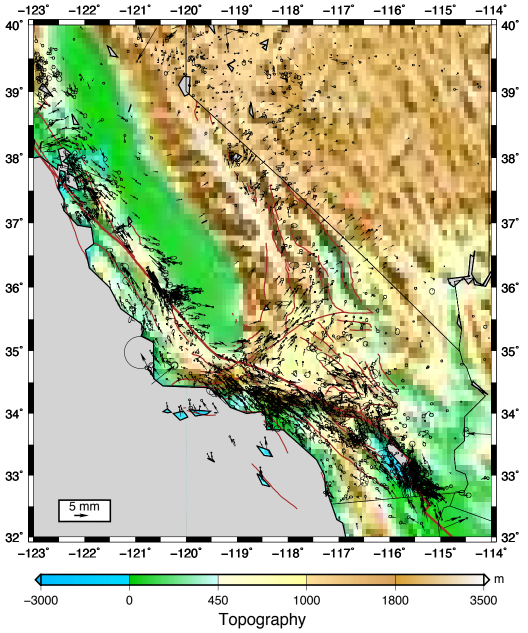

Geodynamic Modeling Vs. Rheological Modeling

Flow laws from Hirth et al. (2001) (quartzite), Rybacki et al. (2006) (feldspar) Kronenberg et al. (1990) (biotite) and Hirth and Kohlstedt (2004) (olivine).

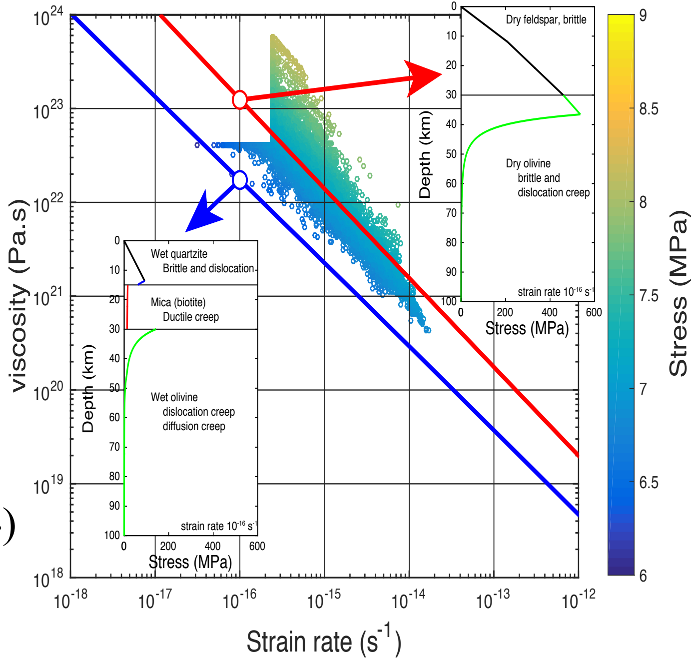

Conclusions

- Our results indicate GPE gradients originating from high paleotopography dominated the extensional stress field prior to and during core-complex formation.
- Dramatic weakening of the lithosphere viscosity accompanied the collapse. Some regions have experienced rheological hardening.
- The most likely weakening influence is heat and fluids associated with slab rollback and volcanism.
- The 45° rotation of extension directions between Miocene to present-day can be explained by the increasing importance of Pacific-North America relative plate motions
- Present-day rheology in Southern California is consistent with intermediate mix between dry and wet end-members

Present-day Seismic Velocity Constraints for Upper Mantle Temperature and Viscosity Variations

$$Vs = \sqrt{\frac{\mu}{\rho}}$$

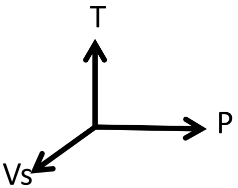

- Shear modulus and upper mantle density are both a function of temperature and pressure .
- Using calculated pressures in WUS for each 0.5 km depth (Moho to 100 km) and a reference dataset for pressure, temperature and Vs (Goes et al., 2000) we determine the temperatures for each specific depth.
- Using the method of Wu et al. (2013) the depth integral of viscosity is computed using the shear velocity data (Shen and Ritzwoller, 2016) and temperature data.

$$\log_{10}(\Delta\eta) = \frac{-0.4343\beta}{[\partial \ln v_s/\partial T]_{ah+an}} \frac{(E^* + pV^*)}{RT_0^2} \frac{\delta v_s}{v_s}$$

Wu et al. (2013)

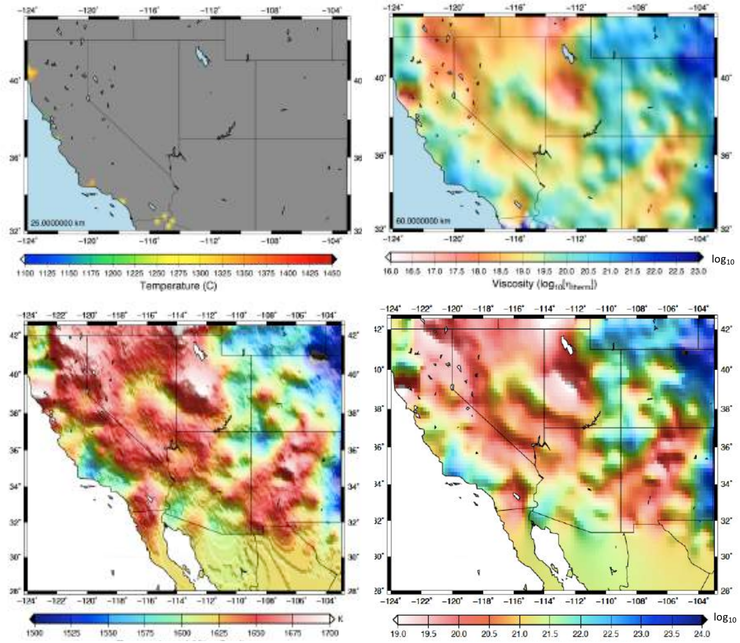

Average temperature from Moho to 100 km. Average viscosity from Moho to 100 km.

The Role of Mantle Fluid Input on Lithospheric Deformation

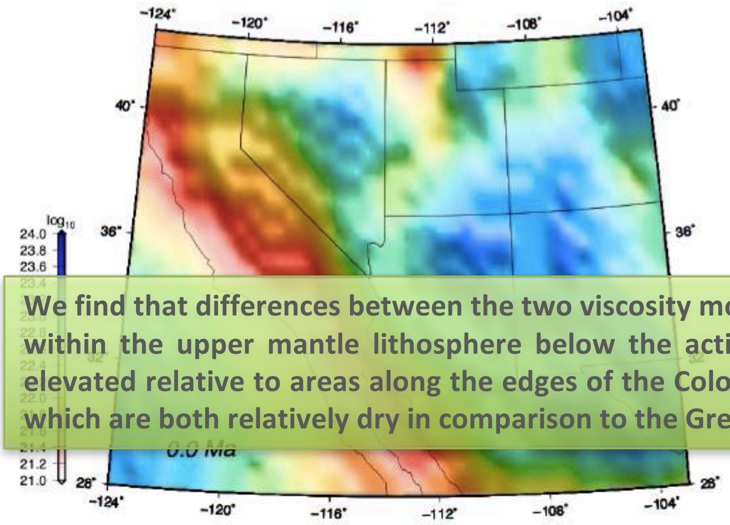

Depth integral of viscosity from geodynamic forward model (Moho to 100 km depth).

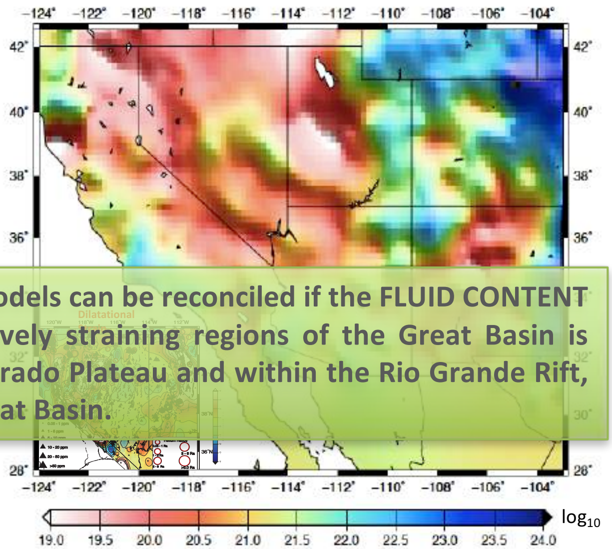

Depth integral of viscosity from seismic shear velocity constraints (Moho to 100 km depth).

We find that differences between the two viscosity models can be reconciled if the FLUID CONTENT within the upper mantle lithosphere below the actively straining regions of the Great Basin is elevated relative to areas along the edges of the Colorado Plateau and within the Rio Grande Rift, which are both relatively dry in comparison to the Great Basin.

Influence of Thermal Perturbations on Western U.S. Upper Mantle Densities

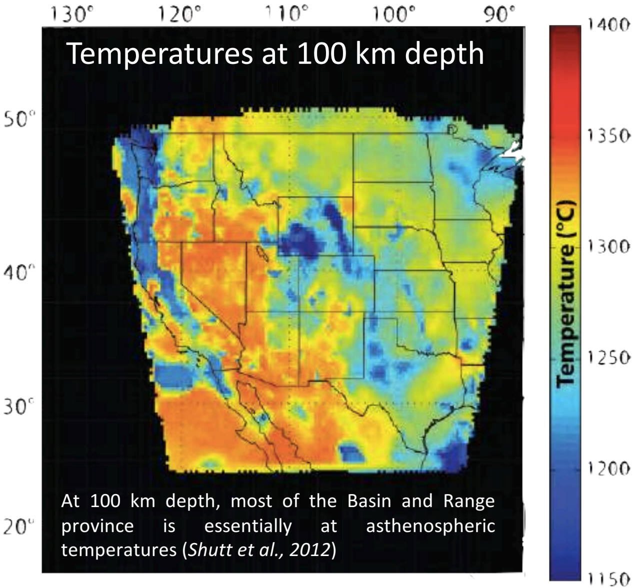

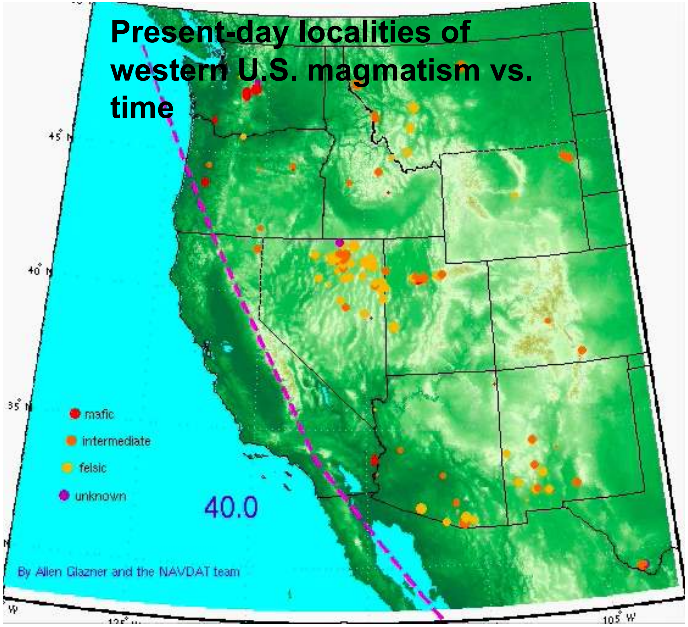

Magmatism in the western U.S. over the past 40 Myrs from *NAVDAT.org*

Lithosphere Foundering of Laramide Flat Subduction and Upper Mantle Temperature Variation

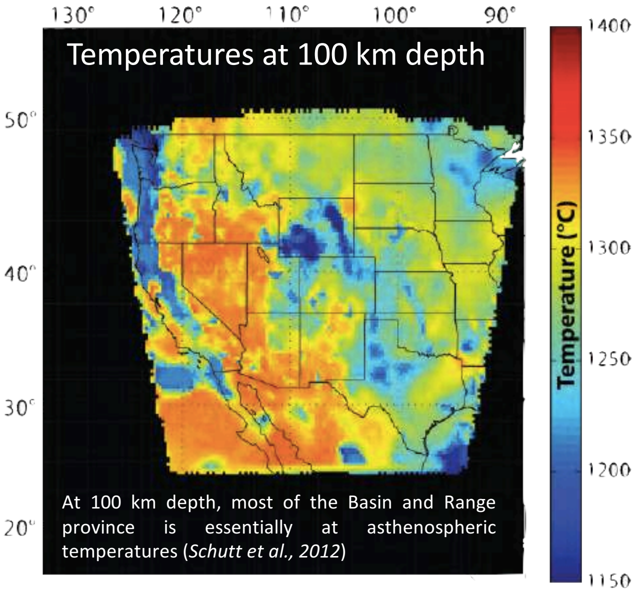

At 100 km depth, most of the Basin and Range province is essentially at asthenospheric temperatures (*Schutt et al., 2012*)

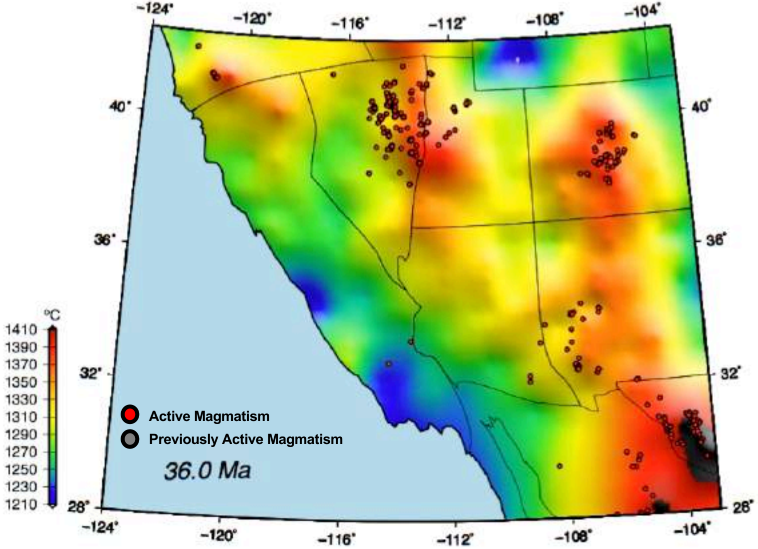

Upper mantle temperature variation in western U.S. from 36 Ma to present-day. Gray dots are the reconstructed position of western U.S. magmatism from *NAVDAT.org*

Upper Mantle Density and Compensation of Topography

Crustal density from seismic velocities after the estimated thermal variations are removed. (*Levandowski et al., 2014*)

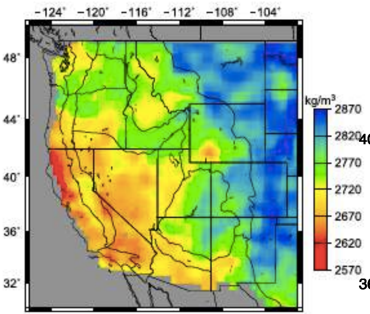

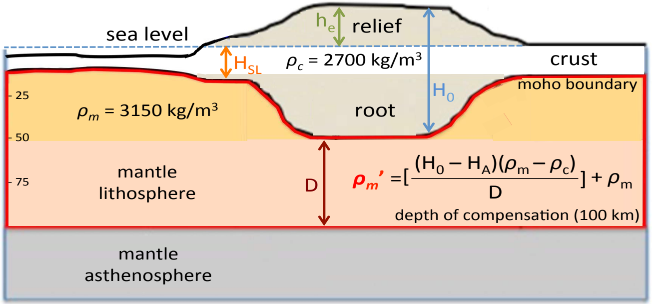

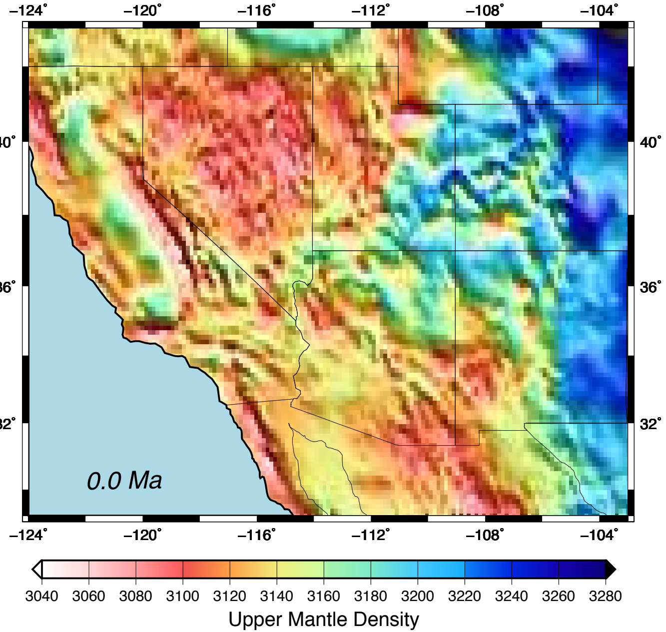

Present-day Upper Mantle Density Model for Western U.S.

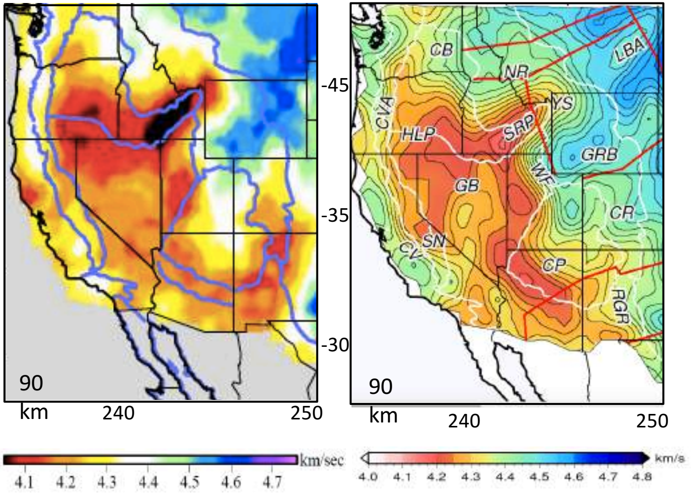

Shear wave speed maps at 90 km depths from *Shen and Ritzwoller (2016)* (left); *Porter et al. (2016)* (right)